THE JOURNAL OF BIOLOGICAL CHEMISTRY VOL. 281, NO. 25, pp. 16879–16887, June 23, 2006

Characterization of the Exchangeable Protons in the Immediate Vicinity of the Semiquinone Radical at the Q_H Site of the Cytochrome bo_3 from *Escherichia coli**

Received for publication, March 17, 2006, and in revised form, April 18, 2006 Published, JBC Papers in Press, April 18, 2006, DOI 10.1074/jbc.M602544200

Lai Lai Yap[‡], Rimma I. Samoilova[§], Robert B. Gennis[‡1], and Sergei A. Dikanov[¶2]

From the [‡]Department of Biochemistry, University of Illinois, Urbana, Illinois 61801, the [§]Institute of Chemical Kinetics and Combustion, Russian Academy of Sciences, Novosibirsk 630090, Russia, and the [¶]Department of Veterinary Clinical Medicine, University of Illinois, Urbana, Illinois 61801

The cytochrome bo_3 ubiquinol oxidase from *Escherichia coli* resides in the bacterial cytoplasmic membrane and catalyzes the two-electron oxidation of ubiquinol-8 and four-electron reduction of O_2 to water. The one-electron reduced semiquinone forms transiently during the reaction, and the enzyme has been demonstrated to stabilize the semiquinone. Two-dimensional electron spin echo envelope modulation has been applied to explore the exchangeable protons involved in hydrogen bonding to the semiquinone by substitution of ^1H_2O by ^2H_2O. Three exchangeable protons possessing different isotropic and anisotropic hyperfine couplings were identified. The strength of the hyperfine interaction with one proton suggests a significant covalent O–H binding of carbonyl oxygen O1 that is a characteristic of a neutral radical, an assignment that is also supported by the unusually large hyperfine coupling to the methyl protons. The second proton with a large anisotropic coupling also forms a strong hydrogen bond with a carbonyl oxygen. This second hydrogen bond, which has a significant out-of-plane character, is from an NH_2 or NH nitrogen, probably from an arginine (Arg-71) known to be in the quinone binding site. Assignment of the third exchangeable proton with smaller anisotropic coupling is more ambiguous, but it is clearly not involved in a direct hydrogen bond with either of the carbonyl oxygens. The results support a model that the semiquinone is bound to the protein in a very asymmetric manner by two strong hydrogen bonds from Asp-75 and Arg-71 to the O1 carbonyl, while the O4 carbonyl is not hydrogen-bonded to the protein.

Cytochrome bo_3 (cyt bo_3)[3] is a terminal oxidase in the aerobic respiratory chain of *Escherichia coli*. It catalyzes the two-electron oxidation of ubiquinol-8 with a semiquinone (SQ) intermediate in an overall reaction that releases two protons to solution. The available evidence suggests that the cyt bo_3 ubiquinol oxidase has two Q binding sites (1–3): a low affinity site (Q_L) where the substrate quinol is oxidized and the product is released, and a high affinity site where the bound quinone species acts as a conduit for electrons, similar to the role of the Q_A site in the bacterial reaction center (3–7, 9). The substrate (QH_2) site, referred to as the low affinity site (Q_L), is equilibrated with the quinone pool in the membrane. The high affinity quinone-binding site (Q_H), from which Q is not readily removed, stabilizes the SQ. The quinone bound at the Q_H site functions as a tightly bound cofactor. Pulse radiolysis studies (10) have shown that the tightly bound quinone can be rapidly reduced to the semiquinone species and that the tightly bound quinone is essential for rapid electron transfer to heme *b*. The first order rate constant for the reduction of heme *b* is $1.5 \times 10^3\ s^{-1}$, which is approximately the turnover rate of the enzyme. It is reasonably assumed that there is a rapid ($>10^4\ s^{-1}$) two-electron reduction of Q_H by the bound substrate Q_LH_2, followed by two one-electron intramolecular transfers from the Q_HH_2 to heme *b*. Hence, the suggested electron transfer sequence is as in Reaction 1.

$$Q_LH_2 \leftrightarrows Q_H \leftrightarrows \text{heme } b \leftrightarrows \text{heme } o_3\text{-}Cu_B \rightarrow O_2$$

REACTION 1

The function of the quinone cofactor bound at the Q_H site as a two-electron/one-electron transformer is supported by the electrochemical studies, which show that the Q_H site stabilizes the SQ form of the quinone bound at this site. The midpoint potential for the two-electron reduction of Q_HH_2 is ~+100 mV at pH 7.5, and the pH dependence (up to pH 9) of the midpoint potential shows that two protons are taken up by the protein upon reduction, probably forming the protonated dihydroubiquinol: $2\ e^{-1} + 2H^+ + Q_H \rightarrow Q_HH_2$.

The midpoint potential for the one-electron oxidation of Q_HH_2 to the SQ species is ~−13 mV, and the pH dependence of the oxidation of the SQ to the fully oxidized quinone indicates oxidation to form the SQ is coupled to the loss of a proton from a group with a pK_a of ~7.5. This has been interpreted as the pK_a of the SQ, predicting that the SQ is an anion ($Q_H^{\cdot-}$) above pH 7.5 but is a neutral species ($Q_H^{\cdot}H$) below pH 7.5 (11).

The x-ray structure of cyt bo_3 (12) does not contain any bound quinone, but site-directed mutagenesis studies (12–15) have identified residues that influence the SQ, resulting in a model for the Q_H binding site (12). This model (12) proposes hydrogen bonds from Asp-75 and Arg-71 to one of the carbonyl oxygens and hydrogen bonds from Gln-101 and His-98 to the second carbonyl oxygen.

Information about the electronic structure of the semiquinone radical in cyt bo_3 and its interaction with the protein environment is available from high resolution EPR studies. The hydrogen-bonded protons around the SQ in cyt bo_3 were previously examined using electron-nuclear double resonance (ENDOR) techniques in conjunction with

* This work was supported by National Institutes of Health (NIH) Grant GM62954 (to S. A. D.), Department of Energy Grant DE-FG02-87ER13716 (to R. B. G.), and National Center for Research Resources/NIH Grant S10-RR15878 for instrumentation. The costs of publication of this article were defrayed in part by the payment of page charges. This article must therefore be hereby marked "*advertisement*" in accordance with 18 U.S.C. Section 1734 solely to indicate this fact.

[1] To whom correspondence may be addressed: Dept. of Biochemistry, University of Illinois, Urbana, IL 61801. Tel.: 217-333-9075; Fax: 217-244-3186; E-mail: r-gennis@uiuc.edu.

[2] To whom correspondence may be addressed: Dept. of Veterinary Clinical Medicine, University of Illinois, Urbana, IL 61801. Tel.: 217-333-3776; Fax: 217-333-8868; E-mail: dikanov@uiuc.edu.

[3] The abbreviations used are: cyt bo_3, cytochrome bo_3 ubiquinol oxidase from *E. coli*; SQ, semiquinone; Q_H, the high affinity quinone-binding site; ESE, electron spin echo; ESEEM, electron spin echo envelope modulation; HYSCORE, hyperfine sublevel correlation; ENDOR, electron-nuclear double resonance; 1D, one-dimensional; 2D, two-dimensional; DFT, density functional theory.

deuterium (D_2O) exchange. The Q-band ENDOR spectrum showed only one splitting from exchangeable deuterium consistent with hydrogen bonding to the quinone oxygen(s) (16). Two pairs of exchange-sensitive features were observed in the X-band ENDOR spectra of cyt bo_3 bound to either native quinone or to exogenously added quinones (17, 18). The data were interpreted by different laboratories as indicating either one H-bonded proton (18) or two equivalent H-bonded protons (17).

A multifrequency (9, 34, and 94 GHz) EPR study was performed with cyt bo_3 bound to ubiquinone-2 selectively labeled with ^{13}C at either the 1- or the 4-carbonyl carbons (19). The EPR spectra revealed significant differences in the hyperfine tensors of these carbons indicating that the radical interacts with the protein in a highly asymmetric manner (19), consistent with a strong hydrogen bond to the O1 carbonyl oxygen. In addition, one- and two-dimensional electron spin echo envelope modulation (1D and 2D ESEEM) studies have shown that the SQ in cyt bo_3 forms an H-bond with a ^{14}N atom from the protein environment (20), tentatively assigned either as coming from the polypeptide backbone (20) or from an arginine side chain (19).

Thus, previous studies have established the presence of at least one H-bond between the SQ in cyt bo_3 and a nitrogen that is part of the protein environment. These results do not exclude additional hydrogen bonds between the quinone oxygens and other protein H-bonding partners, including S and O atoms.

The current work provides additional information about the exchangeable protons in hydrogen bonds to the SQ species in cyt bo_3 by using a combination of 1D and 2D ESEEM, and pulsed ENDOR. The major new observation is that there are at least three exchangeable protons with distinct hyperfine couplings in the immediate environment of the SQ. The data support a model in which the semiquinone is stabilized by strong hydrogen bonds from both Asp-75 and Arg-71 to oxygen O1 and with no hydrogen bonds to carbonyl O4, resulting in a highly asymmetric spin distribution.

EXPERIMENTAL PROCEDURES

Sample Preparation—The pJRHisA plasmid encoding wild-type cyt bo_3 was transformed into the C43(DE3) *E. coli* strain (Avidis, France). Cells were grown in LB medium containing 100 μg/ml ampicillin, 0.3% lactic acid, and 500 μM $CuSO_4$ at 37 °C and harvested at the mid-logarithm phase. Harvested cells were resuspended in 50 mM K_2HPO_4, 5 mM $MgSO_4$, pH 8.3, and broken by passing through a microfluidizer (Microfluidics Corp., Worcester, MA) at 10,000 p.s.i. (three times), followed by centrifugation at 16,000 × *g* for 30 min to remove cell debris. Membranes were then isolated from the supernatant by centrifugation at 180,000 × *g* for at least 5 h. The isolated membranes were suspended in 50 mM K_2HPO_4, pH 8.3, and solubilized with 1% *n*-dodecyl β-D-maltoside (Anatrace, OH) by stirring at 4 °C for 2 h. The unsolubilized material was removed by centrifugation at 15,000 × *g* for 1 h. The solubilized cyt bo_3 was loaded onto a nickel-nitrilotriacetic acid column and purified as described previously (21). The purified protein was then dialyzed overnight in 50 mM K_2HPO_4, 0.1% *n*-dodecyl β-D-maltoside, pH 8.3, and concentrated to ~400 μM. For the deuterated sample, the dialyzed protein was concentrated, exchanged with deuterated 50 mM K_2HPO_4, 0.1% *n*-dodecyl β-D-maltoside, pD 8.3, and further concentrated to ~400 μM. The enzyme was anaerobically reduced under an argon atmosphere with 500-times excess sodium ascorbate, and the reduced sample was then transferred to an argon-flushed EPR tube, followed by rapid freezing in liquid nitrogen.

EPR Measurements—The continuous wave and pulsed EPR experiments were carried out using X-band Bruker ELEXSYS E580 spectrometers equipped with Oxford CF 935 cryostats. Unless otherwise indicated, all measurements were made at 50 K. Several types of ESE experiments with different pulse sequences were employed with appropriate phase-cycling schemes to eliminate unwanted features from experimental echo envelopes. Among them are two-pulse and four-pulse sequences. In the two-pulse experiment ($\pi/2$-τ-π-τ-*echo*) the intensity of the echo signal is measured as a function of the time interval τ between two microwave pulses with turning angles $\pi/2$ and π to generate an echo envelope that maps the time course of relaxation of the spin system (in ESEEM), or as a function of magnetic field at fixed τ (in field-sweep ESE). In the 2D four-pulse ESEEM experiment ($\pi/2$-τ-$\pi/2$-t_1-π-t_2-$\pi/2$-τ-*echo*), also called HYSCORE (22), the intensity of the stimulated echo after the fourth pulse is measured with t_2 and t_1 varied, and τ constant. Such a 2D set of echo envelopes gives, after complex Fourier transformation, a 2D spectrum with equal resolution in each direction. Spectral processing of ESEEM patterns was performed using Bruker WIN-EPR software.

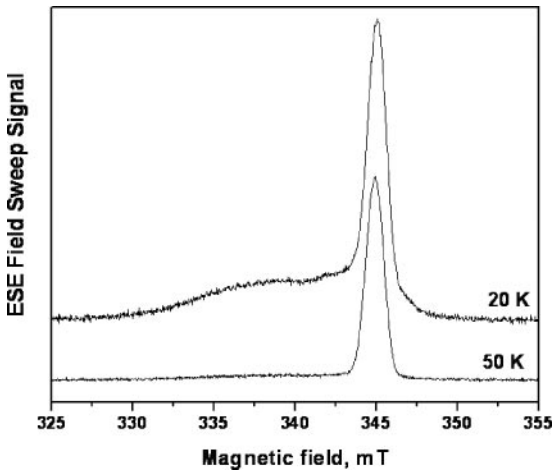

FIGURE 1. **Two-pulse field-sweep ESE spectra of the cyt bo_3 at 20 and 50 K.** The microwave frequency was 9.68 GHz. The spectrum of cyt bo_3 recorded at 20 K (used in previous ESEEM experiments (20)) exhibits a line from the SQ, which is overlapped with another broad, low intensity signal. The broad signal vanished at $T > 40$ K due to shortening of its relaxation times.

Pulsed ENDOR spectra of the radical in cyt bo_3 were obtained using Davies (π-t-$\pi/2$-τ-π-τ) and Mims ($\pi/2$-τ-$\pi/2$-t-$\pi/2$-τ) sequences with different pulse lengths. In addition, radio frequency π pulse is applied during the time interval t in both sequences. The specifics of these experiments are described in detail elsewhere (23).

Characteristics of HYSCORE Spectra from $I = ½$ Nuclei—The most informative experimental data regarding the ligand environment of the semiquinone were obtained from the 2D ESEEM (HYSCORE) experiment (22). The basic advantage of the HYSCORE technique is the creation of 2D spectra with off-diagonal cross-peaks (ν_α, ν_β) and (ν_β, ν_α), whose coordinates are nuclear frequencies from opposite electron spin manifolds. The cross-peaks simplify significantly the analysis of congested spectra by correlating and spreading out the nuclear frequencies. In addition, the HYSCORE experiment separates overlapping peaks along a second dimension and enhances the signal-to-noise ratio through a second Fourier transform. HYSCORE is also valuable for the detection of extended anisotropic peaks of low intensity, which are not seen in 1D ESEEM spectra.

Orientationally disordered (*i.e.* powder) spectra of $I = ½$ nuclei also reveal, in the form of cross-peak contour projections, the interdependence between ν_α and ν_β values in the same orientation. Analysis of the contours allows for direct, simultaneous determination of

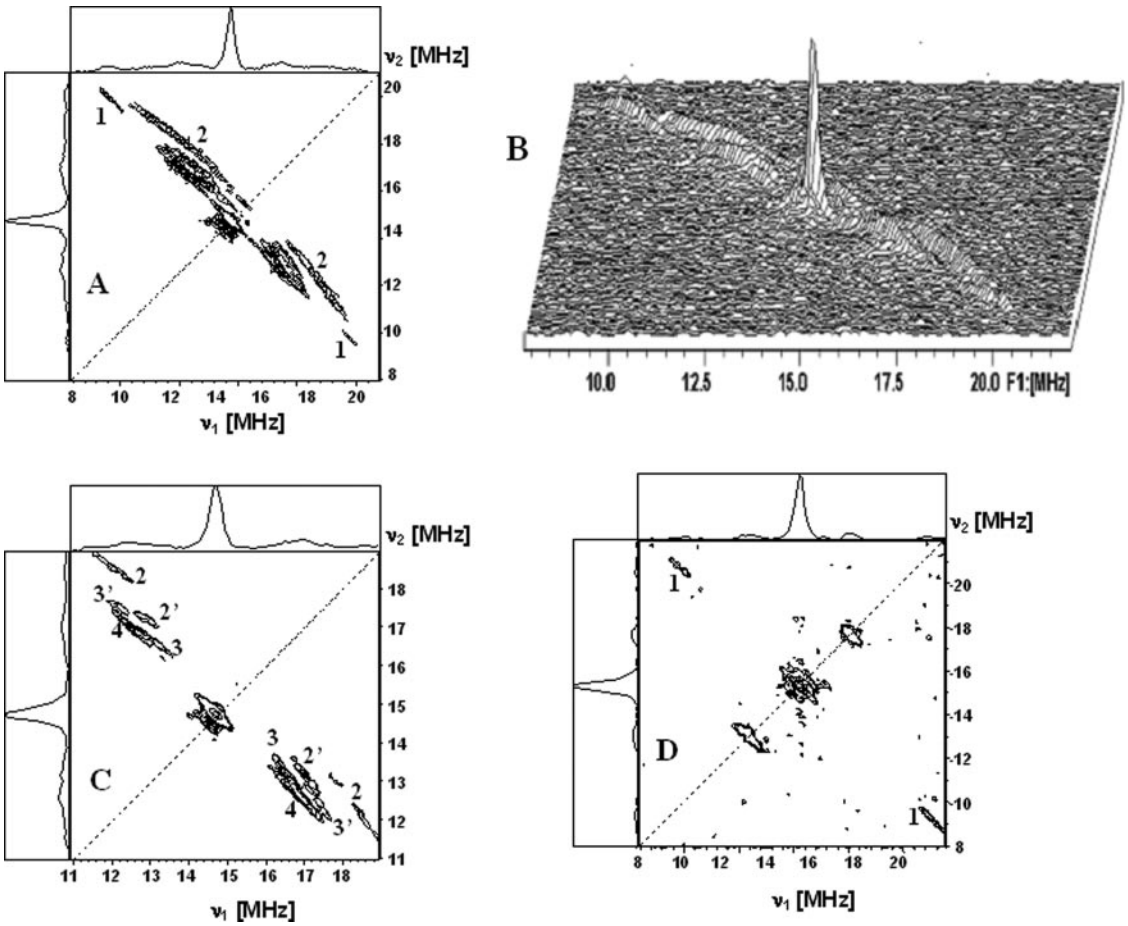

FIGURE 2. **The proton part of the HYSCORE spectra of the SQ at the Q_H site of cyt bo_3.** *A*, *C*, and *D*, contour presentations of the spectra used for the quantitative analysis of lineshapes; *B*, stacked presentation showing more clearly the relative intensities and shapes of the peaks. Spectrum *C* shows higher levels of intensity than spectrum *A*. The microwave frequency was 9.68 GHz, the magnetic field was 345.0 milliteslas, and the time τ between first and second microwave pulses was 136 ns. Spectra were obtained after Fourier transformation of 2D time-domain patterns containing 256 × 256 points with a step of 20 ns.

the nuclear isotropic and anisotropic hyperfine coupling constants (24) (see "Appendix").

RESULTS

EPR and ESEEM Spectra of the Semiquinone—The field-sweep ESE spectrum of cyt bo_3 recorded at 50 K (Fig. 1) shows only one line from the SQ with $g \sim 2.0047$ and the width ~1.2 millitesla at the half-height. Some measurements were also performed at 90 K, and the results were similar to those obtained at 50 K.

The 1D and 2D ESEEM spectra of the SQ at frequencies <10 MHz, appropriate for ^{14}N nuclei, are identical to those reported previously by Grimaldi *et al.* (20). These spectra were used to determine the quadrupole coupling constant $K = e^2qQ/4h = 0.93$ MHz, and the asymmetry parameter $\eta = 0.51$, which are consistent with assigning this to a ^{14}N nitrogen from the NH or NH_2 groups forming an H-bond with the SQ (see "Discussion").

Proton HYSCORE—Fig. 2 (*A–C*) shows the proton part of the HYSCORE spectrum ($\tau = 136$ ns) of the SQ radical in the cyt bo_3 sample prepared in ^1H_2O buffer. In addition to a diagonal peak with extended shoulders at the proton Zeeman frequency ($\nu_H \sim 14.7$ MHz), the spectra in Fig. 2 contain up to six pairs of resolved cross-peaks located symmetrically relative to the diagonal. They are designated **1, 2, 2′, 3, 3′**, and **4**. The cross-peaks labeled **1** demonstrate the largest hyperfine splitting, of the order ~10 MHz. The cross-peaks **2** possess the most extended anisotropic contour in the area further up the diagonal. The peaks **2′, 3, 3′**, and **4** are located in a similar area of the plot close to each other and partially overlap at the low intensity levels. The contours of these peaks could be separated at the higher levels of the intensity, as shown in Fig. 2*C*, and used for quantitative analysis. The **2, 2′, 3**, and **3′** contours deviate from the normal to the diagonal, indicating a significant anisotropic component. In contrast, contours **1** and **4** are approximately normal to the diagonal, suggesting smaller anisotropy. Cross-peaks **2–4** (Fig. 2*D*) completely disappeared in the HYSCORE spectra obtained under the same conditions using the sample with ^2H_2O, showing that these are produced by exchangeable protons. However, cross-peaks **1** and the diagonal peak, with its shoulders, still appear in the spectra.

TABLE 1
Hyperfine tensors of the protons H1–H4 derived from HYSCORE spectra

Proton	a and T	$A_\perp = a - T$	$A_\parallel = a + 2T$
		MHz	
H1	10.0, 1.7	8.3	13.4
H2	±0.7, ∓6.3	±7.0	∓11.9
H3	∓1.2, ±4.2	∓5.4	±7.2
H4	∓4.6, ±1.7	∓6.3	∓1.2

Quantitative analysis of the cross-peak contour lineshapes (see "Appendix") finds that cross-peaks **2** and **2′** are produced by the same proton (H2) and that cross-peaks **3** and **3′** are also from the same proton (H3). Hence, these data derive from four protons coupled to the SQ: H1, H2, H3, and H4. Among them, H2, H3, and H4 are exchangeable pro-

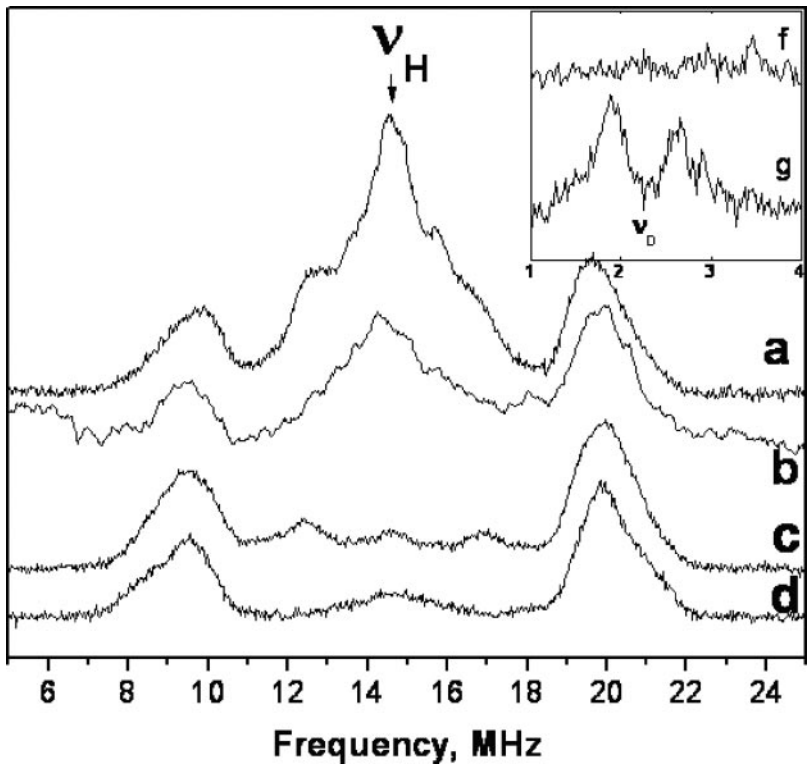

FIGURE 3. **Pulsed ENDOR spectra obtained using Davies ENDOR sequence of the SQ at the Q_H site of cyt bo_3 prepared in ^1H_2O (*a* and *c*) and ^2H_2O (*b* and *d*).** Length of the first inverting microwave π pulse is 240 ns for *a* and *b*, and 64 ns for *c* and *d*. *Inset*, Mims ENDOR spectrum of the SQ in ^1H_2O (*f*) and ^2H_2O (*g*).

tons. The isotropic (a) and anisotropic (T) components of the axial hyperfine tensors for these protons are summarized in Table 1.

Pulsed ENDOR—Fig. 3 shows Davies pulsed ENDOR spectra for the radical in Q_H site of cyt bo_3 prepared in ^1H_2O and ^2H_2O. These spectra were obtained with two different lengths t_p of the inverting π pulse. The spectrum recorded with $t_p = 240$ ns shows complex overlap of the lines in the middle of the spectrum around the proton Zeeman frequency (ν_H). It is seen that the shoulders of this complex line decrease after $^1H/^2H$ exchange. The intensity from the weakly coupled protons around the proton Zeeman frequency is suppressed in the spectra recorded with shorter duration $t_p = 64$ ns. The spectrum in ^1H_2O contains two pairs of peaks located symmetrically relative to the ν_H with splittings of ~11 MHz and ~5 MHz. The pair of peaks with the smaller splitting is absent in the spectrum of the sample prepared in ^2H_2O, thus indicating their assignment to the exchangeable proton(s). In contrast, a new doublet with splitting ~0.73 MHz, centered at the deuterium Zeeman frequency (ν_D) and corresponding to the proton splitting ~5 MHz, appears in these spectra (Fig. 3). One can also note that the shape of the peaks with ~11 MHz splitting also changes in this spectrum due to overlap with some spectral features from exchangeable protons. The shape of these peaks after deuterium substitution becomes more asymmetric, allowing us to specify parallel and perpendicular canonical frequencies with the splittings $|A_\perp| \sim 10$ MHz and $|A_\parallel| \sim 13$ MHz. These features correspond to the cross-peaks from H1 in the HYSCORE spectra, and they are assigned to the methyl protons with the hyperfine couplings shown in Table 1 (see also "Appendix").

The current data can be compared with the results from previous studies. Hastings *et al.* (17) reported two splittings $|A_\perp| = 10.8$ MHz and $|A_\parallel| = 14.4$ MHz (corresponding to $a = 12$ MHz and $T = 1.2$ MHz) that were not sensitive to deuterium exchange in X-band ENDOR spectra of decyl-ubiquinone in the Q_H site of cyt bo_3. These peaks were assigned to the protons of the methyl substituent. MacMillan *et al.* (18) found $|A_\perp| = 9.3$ MHz and $|A_\parallel| = 13.0$ MHz ($a = 10.5$ MHz and $T = 1.2$ MHz) for these protons by pulsed X-band ENDOR of native ubiquinone-8 in cyt bo_3. The most significant loss of intensity after $^1H/^2H$ exchange was reported by these authors at frequencies corresponding to the couplings $|A_\perp| = 5.1$ MHz and $|A_\parallel| = 11.7$ MHz (17) and $|A_\perp| = 4.5$ MHz and $|A_\parallel| = 9.1$ MHz (18). In both of these studies, the features were assigned to the same proton(s) and used for the calculation of the anisotropic component of the hyperfine tensor and H-bond length.

Veselov *et al.* (16) performed orientation-selected Q-band ENDOR experiments with the native SQ in the Q_H site of cyt bo_3. They reported the isotropic coupling of the methyl protons to be ~11 MHz and a loss of intensity in the 4- to 5-MHz region around the proton Zeeman frequency after $^1H/^2H$ exchange. Accordingly, the deuterium ENDOR spectrum recorded at g_y exhibits only one resolved splitting ~0.8 MHz, corresponding to a proton coupling of 5.2 MHz.

In summary, the current work, as well as the previous experiments, have all found a remarkably large anisotropic coupling constant ~10–11 MHz from the methyl protons. In addition, these studies also show similar exchangeable proton and deuterium ENDOR features. Proton ENDOR spectra show a loss of intensity after $^1H/^2H$ exchange, which is most significant at frequencies corresponding to the couplings $|A_\perp| = 4.5$–5.1 MHz and $|A_\parallel| = 9.1$–11.7 MHz.

The powder ENDOR spectrum simulated with the contribution of all three exchangeable protons H2–H4 using the hyperfine tensors given in Table 1 reproduces intense features with a splitting of ~5 MHz resulting from the overlap of lines from all three protons and $|A_\parallel|$ peaks with the splitting ~ 12 MHz from H2 (Fig. 4, "Appendix"). The shape of these features depends on the linewidth of individual ENDOR transitions. Additional factors that may influence the width of these lines in the spectra are the non-axiality of the hyperfine tensors and "strain" in the values of the hyperfine couplings. Thus, the 2D ESEEM data for protons H2, H3, and H4 can explain the exchangeable features in the ENDOR spectra described above, and those data previously assigned

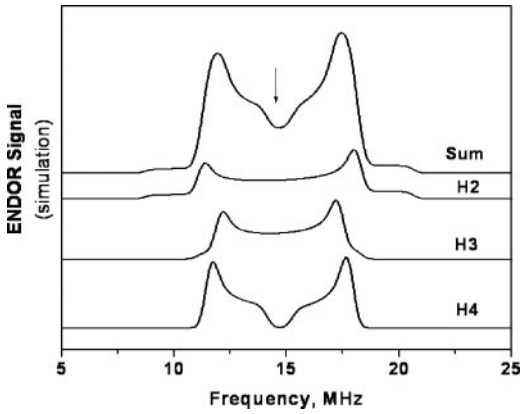

FIGURE 4. **The calculated ENDOR spectra for the protons H2 ($a = \pm 0.7$ MHz, $T = \mp 6.3$ MHz), H3 ($a = \mp 1.2$ MHz, $T = \pm 4.2$ MHz), H4 ($a = \mp 4.6$ MHz, $T = \pm 1.7$ MHz), and sum spectrum.** The individual width of the ENDOR transitions was 0.5 MHz.

by other authors (17, 18) to one or two equivalent H-bonded protons (see "Discussion").

DISCUSSION

A Neutral versus an Anionic Semiquinone—The hyperfine couplings for both the non-exchangeable methyl protons as well for the exchangeable protons obtained from HYSCORE and ENDOR experiments provide several important clues about the nature of the SQ species in cyt bo_3. Previous studies (16–18), along with the current work, have found $a = 10$–11 MHz for the methyl protons. This is the largest isotropic constant reported for these protons for ubiquinones bound to proteins or in solution. Hyperfine coupling of 5.5–6.5 MHz has been reported for ubiquinone anion-radicals in different solvents (25–27). The value changes only slightly in the Q_A and Q_B sites of the photosynthetic reaction center (28). The proton isotropic constant in the rotating methyl group is directly proportional to the π-spin density on the attached carbon atom and described by the McConnel relation $a = 81\rho_\pi$ (29). Thus, the unpaired π-spin density on the carbon attached to the methyl group of the SQ in cyt bo_3 is ~2-fold larger (~7% to ~13%) compared with what is observed with anionic SQ radicals in solution.

In the benzoquinone anion radical, all of the α-protons have an isotropic coupling constant of 6.2 MHz. In contrast, the neutral benzoquinone radical shows two types of α-proton couplings of 13.5 and 1.4 MHz. Similar couplings have been observed for the methyl protons of duroquinone, which is 5.33 MHz in the anion radical but 13.4 MHz and ~1 MHz in the neutral radical. The isotropic coupling constant of the OH proton in these neutral radicals has a value of ~1.5–3 MHz (30). Analogously, the methyl protons of an anion radical of ubiquinone-0 possess an isotropic constant 6.5 MHz, and the corresponding value in the neutral radical with protonated O1 is equal to 12.8 MHz (27). Thus, the data are consistent with the assignment of the SQ bound to the Q_H site being a neutral species (Q·H).

The differences in hyperfine couplings in comparing anionic and neutral SQ radicals result from the protonation of one of the carbonyl oxygens of the semiquinone in the neutral radical, which leads to a shift of spin density and charges within the quinone ring. The bound oxygen possesses a larger negative charge to stabilize the interaction with the proton and, thus, the spin density is partly shifted within the semiquinone. When O1 is protonated, the increase in spin density at carbons C1, C3, C5, and O4 is expected. On the other hand, for O4 protonation, the increase will be seen on atoms C2, C4, C6, and O1 (28). The unpaired π-spin density on the carbon attached to the methyl group of the SQ in cyt bo_3 is entirely consistent with a neutral radical with a protonated O1 oxygen.

The current data also demonstrate three exchangeable protons with significant differences in hyperfine couplings. Two of these protons possess large anisotropic hyperfine couplings with $|T| \sim 4.2$ and 6.3 MHz, which exceed the value $|T| \sim 3$ MHz observed for in-plane hydrogen-bonded protons in alcoholic solutions (25, 31, 32). Recent DFT calculations (33) have shown that the hydrogen-bonded proton with $|T| \sim 3$ MHz corresponds to an O . . . H distance of ~1.8 Å, whereas $|T| = 5.2$ MHz is consistent with 1.4 Å. Hence, the measured coupling of $|T| = 6.3$ MHz requires an even shorter O . . . H bond distance, of the order 1.2 Å, implying substantial covalent character. This result provides additional support for the interpretation that the SQ in cyt bo_3 can be considered not as a hydrogen-bonded anion but as a protonated neutral radical.

Prominent peaks from the β-protons of the isoprenyl tail were not observed in ENDOR and 2D ESEEM. The lack of these features indicates that these protons have small hyperfine couplings and contribute only to the spectral area close to the proton Zeeman frequency. Veselov *et al.* (16) studied these protons in greater detail by using orientation-selected Q-band ENDOR and found that the hyperfine couplings with these protons in the Q_H site (~2–4 MHz) are smaller than for the SQ in solution. This is also consistent with the redistribution of the spin density of the SQ in the Q_H site resulting from the protonation of O1.

Previous studies have shown that the one-electron reduction of the fully oxidized quinone at the Q_H site (Q/Q^-) is coupled to the protonation of a group with a pK_a of ~7.5. If it is the SQ itself that is protonated, this would predict a neutral semiquinone dominating below pH 7.5 ($Q/Q^{\bullet}H$) and an anionic species above pH 7.5 (Q/Q^-). However, the EPR spectra from previous publications (11, 17, 20) show that the large hyperfine coupling of the methyl protons is present from pH 6 to 9. No transition from a neutral radical (large hyperfine coupling to the methyl hydrogens) to a species with characteristics of the anionic radical (smaller hyperfine coupling to the methyl hydrogens) is observed as the pH is increased above pH 7.5. This eliminates the SQ itself as being the protonatable group with a pK_a of 7.5 and indicates that the pH dependence of the E_m of the (Q/SQ) couple is more complicated than previously thought. Pulsed radiolysis experiments have monitored the transient formation of the SQ radical in the Q_H site at pH 7 by ultraviolet absorption (10). The data were interpreted to show an anionic radical being formed based on the absence of a resolved absorption maximum at 420 nm, which is characteristic of a neutral radical. However, the pulse radiolysis data are not compelling and are complicated by the spectrum of the *N*-methyl nicotinamide radical generated as the reductant in these experiments. As already pointed out, the EPR spectra in the current work are not compatible with an anionic SQ species, although the transient species may not be identical to the stabilized form of the SQ.

Comparison with Recent DFT Calculations—DFT calculations can be used to provide insight into the detailed relations between the structure, environment, and EPR characteristics of the ubisemiquinone radical. A recent study (34) modeled the SQ bound to the Q_H site of cyt bo_3, calculating the *g*-tensor and the ^{13}C, ^{1}H, and ^{17}O hyperfine tensors with the assumption that the SQ is an anionic species and testing a variety of H-bonding schemes.

The calculation performed optimized the SQ-protein complex considered as an anion-radical involved in the hydrogen bonds with oxygen and nitrogen atoms. The O . . . H bond lengths in the optimized structures were varied between 1.75 and 2.12 Å for the protons H-bonded to O1 and O4 for the different models of the complex. It was concluded that a single-sided binding model cannot account for the experimentally observed *g*-tensor nor for the asymmetry of the ^{13}C carbonyl hyperfine tensors. A model with two hydrogen bonds to O1 and one hydrogen

bond to O4 (2-1 model) was suggested for the Q_H site, but a model with one more hydrogen bond on each side (3-2 model) could not be excluded.

The model proposed is in agreement with our observation of three exchangeable protons around the SQ. However, the calculated hyperfine couplings with H-bonded protons (34) are inconsistent with the experimental values determined in the current work. The components of the calculated hyperfine tensors with 2.5 MHz $< |T| <$ 4 MHz are systematically lower than those found for H2 and H3. The low values of the calculated hyperfine tensors result from the H-bond lengths considered in the model. The experimental coupling of the third H-bond in the current work (H4) is smaller than the calculated values, which leaves doubt as to whether this H-bond is to either of the carbonyl oxygens.

An important discrepancy between the calculations of the favored 2-1 model (34) and the experimental data is that the calculations predict the isotropic coupling with the methyl protons to be only 6–7 MHz, compared with the measured values near 10–11 MHz. Better agreement is found with the 2-0 model, which predicts coupling of ~9 MHz.

The *g*-tensor calculations systematically yield higher g_x value for all models of coordination than experimentally observed. The authors note that the "artificial" shortening of hydrogen bonds to 1.6 Å in the 2-1 model reduce the value of g_x, but this case is excluded as "very unlikely," although the model with one shortened H-bond to oxygen O1 provides good agreement with the ^{13}C experimental values.

The experimental data presented in the current work, however, strongly support a model with a short H-bond to oxygen O1, *i.e.* an O–H bond with significant covalent character. It is likely that a more satisfactory description of the EPR parameters could be obtained by considering the SQ to be a neutral radical.

Non-planarity and Exchangeable Protons H2 and H3—In proteins, one factor influencing the geometry of hydrogen bonds and proton hyperfine couplings is the structure of the quinone-processing site, particularly the location of suitable hydrogen-bond partners for the semiquinone oxygens. As a result, the hydrogen bonds are likely forced either above or below the ring plane. The DFT calculations show that deviation of the hydrogen bond from the quinone plane leads to a simultaneous increase of the isotropic and anisotropic coupling of the hydrogen-bonded proton (35). This demonstrates the importance of the H-bond geometry in determining the magnitude of the H-bond tensor. This effect is not accounted for in the simple point-dipole model used for estimation of H-bond length. This geometry factor can be considered as an alternative explanation of the large hyperfine values found for the two exchangeable protons and reinforces their assignment to the protons of hydrogen bonds with the carbonyl oxygens. It is important, however, that H-bond deviation does not influence the hyperfine couplings with the ring protons (35) and thus cannot explain the increase of the couplings with methyl protons. The calculations also predict a significant increase of the isotropic hyperfine coupling for the out-of plane protons that is contradicted by the hyperfine coupling ~0.7 MHz selected for H2. Therefore, the out-of-plane deviation cannot explain simultaneously the hyperfine coupling for H2 and large methyl proton couplings as can be done by invoking a covalent O–H bond to the O1 oxygen in the SQ. However, the characteristics of the exchangeable proton H3 with $|a| = 1.2$, and $|T| = 4.2$ MHz can be explained by the formation of the out-of-plane H-bond. In DFT calculations, similar characteristics were obtained for the out-of-plane deviation ~45° of the H-bond with typical in-plane characteristics, *i.e.* $a \sim 0$ and $|T| = 3$ MHz (35).

The Nature of H-bonded Nitrogen—Based on the crystal structure, it was proposed (12) that the carbonyl oxygens of the bound ubiquinol can form up to four hydrogen bonds with the protein, to Asp-75, Arg-71, His-98, and Gln-101. Site-directed mutagenesis studies (12, 13) have confirmed that these four residues are functionally important and that mutants at each position alter or eliminate the SQ that is stabilized at the Q_H site (13). Hence, there are three potential hydrogen bonds in the proposed model with nitrogen atoms: Arg-71, His-98, and Gln-101.

Grimaldi *et al.* (20) initially assigned the quadrupole parameters $K =$ 0.93 MHz and $\eta = 0.51$ for the H-bonded ^{14}N observed in the ESEEM spectra to an amide (peptide) backbone nitrogen –NH–C=O. The following publication from the same laboratory (19) noted that the nitrogen of an arginine residue cannot be excluded as a possible ligand, as suggested by the proposed structure of the Q_H site in cyt *bo*$_3$. However, the arguments for such assignment were not provided.

The amide nitrogen in free peptides, such as in metal complexes of diglycine and H-bonded to sulfur atoms of iron-sulfur clusters (36–40), has a narrow range of quadrupole coupling constants, $K = 0.75–0.85$ MHz, determined by the electronic structure and the geometry of the planar peptide group; this coupling constant is only slightly perturbed by hydrogen bonding. This has been confirmed by the calculations of the quadrupole coupling tensor (39, 41, 42). The quadrupole constant *K* for nitrogen in cyt *bo*$_3$ slightly exceeds the *K* values reported for peptide nitrogens in different compounds. The assignment by Grimaldi *et al.* (see Fig. 5 in Ref. 20) is based on the comparison with quadrupole coupling constants of peptide nitrogens in model compounds and nitrogens at the Q_A site of the reaction centers (43, 44) and the Q_A site in photosystem II (45) involved in H-bonding with quinones and assigned to peptide nitrogens. Importantly, however, the *K* values in these cases are all in the range 0.75–0.85 MHz, *i.e.* they are systematically lower than the *K* value in cyt *bo*$_3$.

Higher values of the $K \sim 0.9–1.0$ MHz have been reported for the NH_2 group in primary aliphatic and aromatic amines and amides (46), and for the substituent in nitroxide radicals in frozen alcohol solutions (8). Available experimental data also do not allow the NH group to be excluded as a possible donor of the H-bond (46). Hence, the ^{14}N seen in the ESEEM spectra of the quinone radical in the Q_H site could, indeed, be from an NH_2 or NH group of the Arg-71 side chain.

The initial model of the Q_H binding site (12) also predicts hydrogen bonds to the nitrogen atoms from His-98 and Gln-101. The quadrupole characteristics of the ^{14}N detected in ESEEM spectra could not belong to any imidazolate nitrogen of a histidine residue, which exhibit significantly smaller *K* values. A hydrogen bond to His-98 can be rigorously excluded based on these data. The remaining possibility, which is consistent with the structural model (12), is a hydrogen bond between the -NH_2 group of Gln-101 and the O4 carbonyl atom.

Model of the SQ Environment—The current data report three differently coupled exchangeable protons around the SQ in cyt *bo*$_3$. One of the protons requires a very short O . . . H, strongly indicating that the SQ species is a neutral radical. Of particular interest is the previously reported D75H mutant that, though enzymatically inactive, stabilizes the SQ with the same midpoint potential as does the wild-type enzyme (13). However, the EPR spectrum of the D75H mutant does not possess the hyperfine structure resulting from the large hyperfine coupling to the methyl protons (13). This suggests that the D75H mutant stabilizes the anionic form of the SQ. Hence, it is proposed that H2 is a hydrogen bond from Asp-75 to oxygen O1, which has covalent character, resulting in the neutral radical at the Q_H site.

The excess of negative spin density on O1 resulting from the strong (covalent) H-bond with Asp-75 facilitates the formation of the second hydrogen bond by proton H3 ($|a| = 1.2$ MHz, $|T| = 4.2$ MHz) between

O1 and a nitrogen donor from Arg-71 observed in ESEEM spectra. These two protons, H2 and H3, stabilize the strong asymmetry in the distribution of the unpaired spin density that is observed.

Currently, one can propose several structural possibilities for H4. It can be the second proton of the -NH_2 group not participating in H-bond with the SQ but involved in magnetic interaction with the unpaired electron spin. Unpaired spin density transfers on this proton via the bridge O . . . H–N–H. Also H4 could come from the formation of a hydrogen bond to the oxygen of a methoxy group, which would be expected to possess a significantly smaller unpaired spin density than found on the carbonyl oxygen. Alternatively, H4 could be a proton at a second shell distance.

Clearly, further work is needed to clarify the situation. However, the data presented in the current work are by far the most definitive by directly addressing the characteristics of hydrogen bonds for the SQ stabilized at the Q_H site.

CONCLUSION

The present study reports for the first time the finding of three exchangeable protons with different hyperfine couplings in the environment of the SQ species in Q_H site of cyt bo_3 quinol oxidase. The analysis of the hyperfine couplings with methyl protons of the SQ and exchangeable protons allows several conclusions about the nature of the SQ and the structure of its environment as follows. 1) The SQ stabilized by cyt bo_3 at the Q_H site possesses the characteristics of a neutral radical. The data suggest significant covalent character of the O–H bond of carbonyl oxygen O1. This is supported by the unusually large hyperfine coupling to the methyl protons and one exchangeable proton. The exchangeable proton is shared between Asp-75 and O1 oxygen of the SQ. 2) A second exchangeable proton is shared between carbonyl oxygen O1 and a nitrogen-containing group of Arg-71. 3) A third exchangeable proton is weakly coupled to the SQ electron spin and is not involved to the direct binding with carbonyl oxygens. 4) It is proposed that there is one-sided binding of the semiquinone to the protein via O1, supporting the previous conclusion by Grimaldi *et al.* (19), based on the analysis of the ^{13}C couplings of carbonyl carbons. Hence, there is a highly asymmetric binding of the SQ in the Q_H site of cyt bo_3, ruling out the hypothesis by Hastings *et al.* (17) that postulates a binding site with two equivalent hydrogen bonds.

Acknowledgment—We are grateful to Dr. F. MacMillan for providing us with reference 34 prior the publication.

APPENDIX

Analysis of HYSCORE Spectra—The contour lineshape in the powder 2D spectrum from the ^1H nuclei (nuclear spin I = ½, Zeeman frequency ν_I) for axial hyperfine interactions is described (27) by Equation 1.

$$\nu_\alpha = \{Q_\alpha \nu_\beta^2 + G_\alpha\}^{1/2} \quad \text{(Eq. 1)}$$

where

$$Q_\alpha = \frac{T + 2a - 4\nu_I}{T + 2a + 4\nu_I} \quad \text{(Eq. 2)}$$

and

$$G_\alpha = 2\nu_I\left(\frac{4\nu_I^2 - a^2 + 2T^2 - aT}{T + 2a + 4\nu_I}\right) \quad \text{(Eq. 3)}$$

For each cross-peak contour, the frequency values along the ridge can be plotted as $\nu_\alpha{}^2$ *versus* $\nu_\beta{}^2$, transforming the contour lineshape into a straight line segment whose slope and intercept are proportional to Q_α and G_α, respectively. These values can then be used to obtain two possible solutions of isotropic (a) and anisotropic (T) couplings with the same value of $|2a+T|$ and interchanged $A_\perp = |a - T|$ and $A_\parallel = |a + 2T|$ (24).

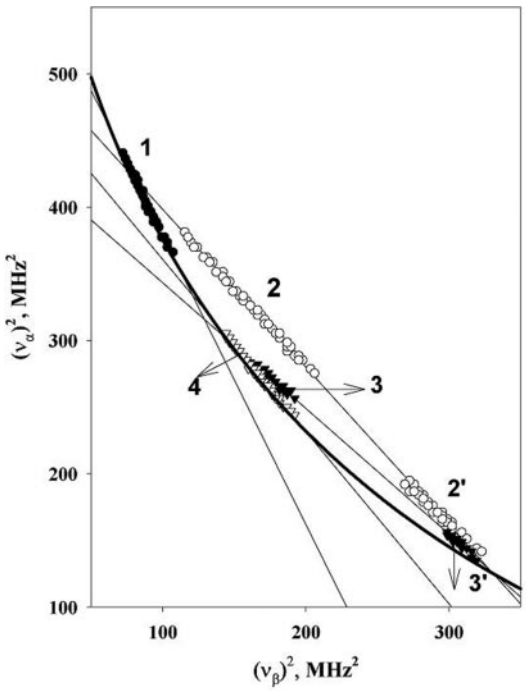

FIGURE 5. **Plots of cross-peaks 1, 2, 2′, 3, 3′, and 4 from HYSCORE spectra measured at several different times in the $\nu_\alpha{}^2$ *versus* $\nu_\beta{}^2$ coordinate system (see text for detailed explanations).** The *straight lines* show the linear fit of plotted data points. The *thick curved line* is defined by $|\nu_\alpha + \nu_\beta| = 2\nu_I$, with a proton Zeeman frequency of 14.689 MHz.

The coordinates ν_α and ν_β of arbitrary points along the ridge formed by the uppermost contour for each proton cross-peak **1**–**4** were measured from HYSCORE spectra recorded with different τ values at a constant magnetic field value and plotted as sets of values for $\nu_\alpha{}^2$ *versus* $\nu_\beta{}^2$. Initially, the larger frequency of each point was arbitrarily selected as ν_α, and the smaller as ν_β for all cross-peaks. The points have been fitted by linear regression to give the slopes and intercepts. In this presentation we have found that the slopes of the linear regression for the **2** and **2′** lines have an inverse relationship, *i.e.* Q_α (**2**) ≅ 1/Q_α (**2′**). This means that the **2′** peak is produced by the same proton H2 but belongs to the cross-feature with opposite assignment of the nuclear frequencies, *i.e.* ($\nu_\beta > \nu_\alpha$) instead of ($\nu_\alpha > \nu_\beta$) (24). In other words, **2** and **2′** are parts of the same cross-feature located on different sides relative to the diagonal of (++)-quadrant (see also Fig. 6). A similar relation between slopes Q_α (**3**) ≅ 1/Q_α (**3′**) was observed for cross-peaks **3** and **3′**, thus indicating that they are produced by the same proton H3.

Fig. 5 shows the plot where the smaller coordinates for cross-peaks **2′** and **3′** were assigned to ν_α and larger ones to ν_β, in contrast to peaks **1,2,3,4**. In such a presentation, the points from **2** and **2′** fit the linear regression well, thus confirming their assignment to the proton, H2. The same is true for peaks **3** and **3′** produced by proton H3. Peaks **1** and **4** result from proton(s) H1 and H4. The slopes and intercepts for the linear regressions shown in Fig. 5 are presented in Table 2, together with two possible sets of (a and T) satisfying Equation 1 for protons H1–H4, and $A_\perp$ and $A_\parallel$ values.

In addition to the experimental points, the curve $|\nu_\alpha + \nu_\beta| = 2\nu_I$

TABLE 2
Parameters derived from contour lineshape analysis of HYSCORE spectra

Proton	Q_α	G_α	(a and T)[a]	$A_\perp = a - T$	$A_\parallel = a + 2T$
		MHz^2		*MHz*	
H1	−2.17 (0.03)	595.98 (2.77)	∓11.7, ±1.7	∓13.4	∓8.3
Peaks **1**			**∓10.0, ∓1.7**	**∓8.3**	**∓13.4**
H2	−1.18 (0.01)	516.78 (0.88)	∓5.6, ±6.3	∓11.9	±7.0
Peaks **2** and **2′**			**±0.7, ∓6.3**	**±7.0**	**∓11.9**
H3	−0.94 (0.03)	437.89 (4.47)	**∓1.2, ±4.2**	**∓5.4**	**±7.2**
Peaks **3** and **3′**			±3.0, ∓4.2	±7.2	∓5.4
H4	−1.29 (0.02)	489.89 (2.79)	**∓4.6, ±1.7**	**∓6.3**	**∓1.2**
Peaks **4**			∓2.9, ∓1.7	∓1.2	∓6.3

[a] The analysis described in the text provides only relative signs of a and T values. For both a and T, the signs given in this table can be exchanged so as to correspond to the opposite assignments (larger frequency of the proton cross-peak to ν_β and smaller one to ν_α). Because of this uncertainty, this table shows all possible signs for each set (a and T), and corresponding $A_\perp = a - T$, and $A_\parallel = a + 2T$.

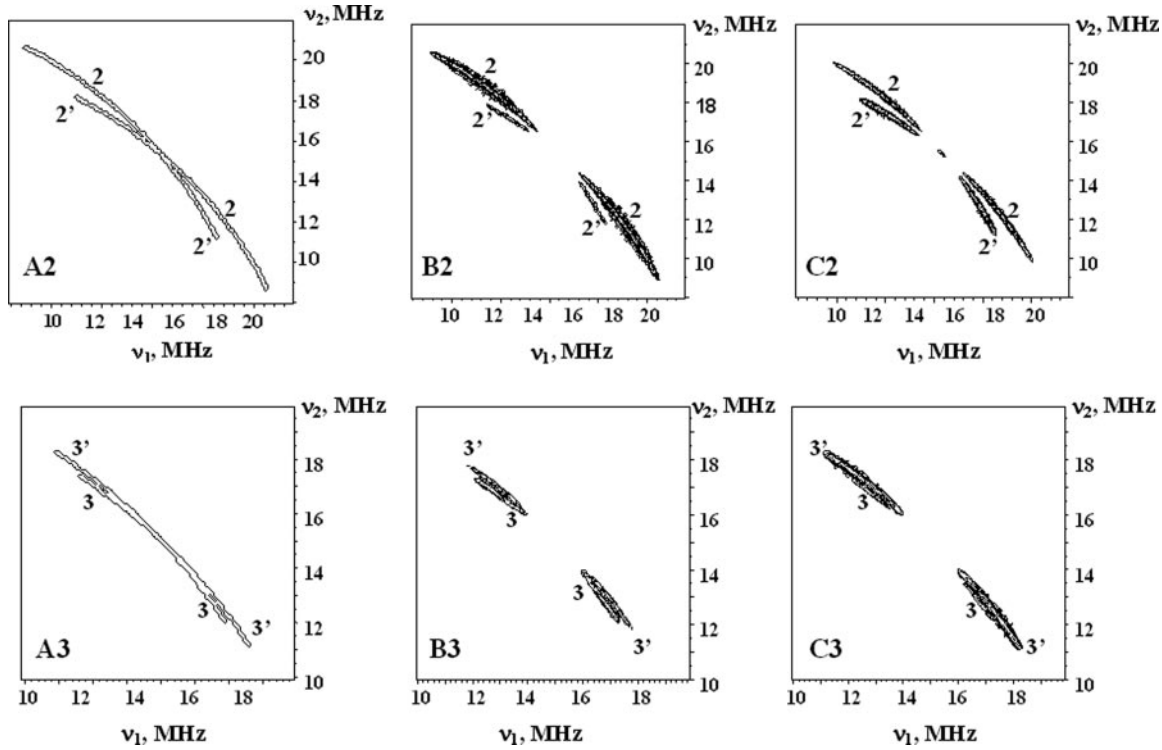

FIGURE 6. **The calculated HYSCORE spectra for protons H2 (*A2–C2*) and H3 (*A3–C3*).** *A2* and *A3* represent an ideal contour presentation for the cross-peaks from H2 and H3, respectively. This presentation is similar for both sets of (*a* and *T*) shown in Table 2 for each proton. *B2* is the calculated HYSCORE spectrum ($\tau = 136$ ns) for H2 with $a = \mp 5.6$ MHz; $T = \pm 6.3$ MHz. *B3* is the calculated HYSCORE spectrum ($\tau = 136$ ns) for H2 with $a = \pm 0.7$ MHz; $T = \mp 6.3$ MHz. *C2* is the calculated HYSCORE spectrum ($\tau = 136$ ns) for H2 with $a = \mp 1.2$ MHz; $T = \pm 4.2$ MHz. *C3* is the calculated HYSCORE spectrum ($\tau = 136$ ns) for H2 with $a = \pm 3.0$ MHz; $T = \mp 4.2$ MHz. Spectra qualitatively demonstrate the relative intensity of different ridges. The wider and more extended ridges possess greater intensity.

(using $\nu_I = 14.689$ MHz corresponding to the proton Zeeman frequency in the field 345 milliteslas) is plotted in Fig. 5 to explain the nature of the two solutions determined by Equation 1. The points at which the curve crosses each extrapolated straight line correspond to the nuclear frequencies ν_α and ν_β at canonical orientations. For an axial hyperfine tensor, there are two possible assignments of the parallel or perpendicular orientations and consequently, two sets of hyperfine tensors, one for each assignment. This approach gives hyperfine couplings identical to those determined from the slope and intercept.

The Hyperfine Couplings of Protons—Selection of the right (a and T) for protons **1–4** from the two alternatives (Table 2) is based on the simulation of the HYSCORE spectra and/or comparison with the ENDOR data. The cross-peaks in HYSCORE spectra possess a maximum at some intermediate frequencies with zero intensity in the canonical orientations of the hyperfine tensor, and the spectra simulated for two possible sets do not always provide convincing support for any of them. This was the situation for the simulated spectra from H1 and H4.

Selection of the preferred set (a and T) for H1 was made on the basis of the ENDOR data. Of the two sets found for H1 from the HYSCORE spectra, the set with $a = \mp 10.0$ MHz, and $T = \mp 1.7$ MHz gives $|A_\perp| = 8.5$ MHz and $|A_\parallel| = 14.0$ MHz, which are reasonably close to the couplings $|A_\perp| \sim 9.3$–10.5 MHz and $|A_\parallel| = 13$–14.0 MHz observed in ENDOR spectra in this and previous reports (17, 18). This set marked by bold font in Table 2 is selected as a correct combination. Thus, we assign cross-peaks **1** to the protons H1 of the methyl group with the couplings $a = 10$ MHz, and $T = 1.8$ MHz. The choice of absolute signs follows from the *triple* ENDOR experiments (25, 26).

The preferred set for protons H2 and H3 are found from the simulation of HYSCORE spectra. Fig. 6 shows the ideal contour presentation of the cross-peaks (Fig. 6, *A2* and *A3*) and the calculated HYSCORE spectra with $\tau = 136$ ns for two sets of (a and T) from Table 2 (Fig. 6, *B2* and *B3*, and *C2* and *C3*). The contour presentation of the spectrum for each proton is identical for both sets. This shows that cross-peaks of these protons are extended ridges located at both sides relative to the

diagonal of the 2D spectrum. Two ridges cross at the diagonal. They are located close to each other, especially for H3. However, the calculated spectra develop significant differences between the two sets in the distribution of the intensity over the parts of the ridges located on different sides of the diagonal. In agreement with the experiment, the intensity is suppressed in the area around the diagonal in the calculated spectra. This effectively leads to the appearance of the two isolated cross-peaks, which can be correlated to each other using a linear regression approach. For H2, the intensity of part **2** significantly exceeds the intensity of part **2′** for one set (Fig. 6). For the second set, the intensities of part **2′** and **2** are comparable. This behavior is in better correspondence with the experimental spectra (Fig. 2, *A* and *B*), which allows us the assignment of $a = \pm 0.7$, $T = \mp 6.3$ MHz set to H2. The intensity of the ridges **3** and **3′** in simulated HYSCORE spectra for H3 is in better agreement with experiment for $a = \mp 1.2$ MHz, $T = \pm 4.2$ MHz.

ENDOR spectra, show a loss of intensity after $^1H/^2H$ exchange, which is most significant at frequencies corresponding to the couplings $|A_\perp| =$ 4.5–5.1 MHz and $|A_\parallel| =$ 9.1–11.7 MHz. The HYSCORE analysis has not identified the exchangeable proton with$|A_\perp|$and $|A_\parallel|$ simultaneously matching these two features. On the other hand, among selected sets, only $|A_\parallel| =$ 11.9 MHz of H2 corresponds to the $|A_\parallel| =$ 9.1–11.7 MHz. The HYSCORE data show that the signs of $A_\perp$ and $A_\parallel$ for H2 and H3 are opposite. This means that the spectral lines corresponding to the two electron spin manifolds for each of these protons overlap in the frequency interval from $-|A_\perp|/2$ to $+|A_\perp|/2$ around the proton Zeeman frequency, producing the enhanced intensity in the center of spectrum between the intensity maxima at $\pm|A_\perp|/2$ (Fig. 4). The $|A_\perp|/2$ for H2 and H3 equal to 3.5 and 2.7 MHz, respectively, and the intervals of enhanced intensity almost coincide.

The simulations of HYSCORE spectra for H4 do not lead to a convincing identification of the preferred set. The ENDOR spectra suggest the appearance of the $|A_\perp|/2 = 3.1$ MHz peaks for $a = \mp 4.6$ MHz and $T = \pm 1.7$ MHz, *i.e.* located between the $|A_\perp|/2$ lines from H2 and H3, that would probably produce the single maximum from the overlap of $|A_\perp|/2$ features from three different protons. Indeed, the simulated ENDOR spectrum with the contribution of all three protons demonstrates intense features with a splitting of ~5 MHz resulting from the overlap of lines from all three protons and $|A_\parallel|$features with the splitting ~12 MHz from H2 (Fig. 4). The shape of these features depends on the linewidth of individual ENDOR transitions. The second possibility for H4 predicts the appearance of $|A_\perp|$ peaks with the splitting ~1 MHz. However, we, as well as others (17, 18), do not find convincing evidence for such splitting when comparing ENDOR spectra of the samples prepared in ^1H_2O and ^2H_2O.

These considerations show that by using HYSCORE data for the three exchangeable protons, one can explain features in the ENDOR spectra previously assigned by other authors (17, 18) to one or two equivalent H-bonded protons.

REFERENCES

1. Sato-Watanabe, M., Mogi, T., Ogura, T., Kitagawa, T., Miyoshi, H., Iwamura, H., and Anraku, Y. (1994) *J. Biol. Chem.* **269,** 28908–28912
2. Sato-Watanabe, M., Mogi, T., Sakamoto, K., Miyoshi, H., and Anraku, Y. (1998) *Biochemistry* **37,** 12744–12752
3. Musser, S. M., Stowell, M. H. B., Lee, H. K., Rumbley, J. N., and Chan, S. I. (1997) *Biochemistry* **36,** 894–902
4. Sato-Watanabe, M., Mogi, T., Miyoshi, H., and Anraku, Y. (1998) *Biochemistry* **37,** 5355–5361
5. Osborne, J. P., Musser, S. M., Schultz, B. E., Edmondson, D. E., Chan, S. I., and Gennis, R. B. (1998) in *Oxygen Homeostasis and Its Dynamics* (Ishimura, Y., Shimada, H., and Suematsu, M., eds) pp. 33–39, Springer-Verlag, Tokyo
6. Puustinen, A., Verkhovsky, M. I., Morgan, J. E., Belevich, N. P., and Wikström, M. (1996) *Proc. Natl. Acad. Sci. U. S. A.* **93,** 1545–1548
7. Mogi, T., Sato-Watanabe, M., Miyoshi, H., and Orii, Y. (1999) *FEBS Lett.* **457,** 223–226
8. Dikanov, S. A., and Tsvetkov, Yu. D. (1992) *Electron Spin Echo Envelope Modulation (ESEEM) Spectroscopy*, CRC Press, Boca Raton, FL, pp. 198–199
9. Schultz, B. E., Edmondson, D. E., and Chan, S. I. (1998) *Biochemistry* **37,** 4160–4168
10. Kobayashi, K., Tagawa, S., and Mogi, T. (2000) *Biochemistry* **39,** 15620–15625
11. Ingledew, W. J., Ohnishi, T., and Salerno, J. C. (1995) *Eur. J. Biochem.* **227,** 903–908
12. Abramson, J., Riistama, S., Larsson, G., Jasaitis, A., Svensson-Ek., M., Laakkonen, L., Puustinen, A., Iwata, S., and Wikström, M. (2000) *Nat. Struct. Biol.* **7,** 910–917
13. Hellwig, P., Yano, T., Ohnishi, T., and Gennis, R. B. (2002) *Biochemistry* **41,** 10675–10679
14. Hellwig, P., Barquera, B., and Gennis, R. B. (2001) *Biochemistry* **40,** 1077–1082
15. Hellwig, P., Mogi, T., Tomson, F. L., Gennis, R. B., Iwata, J., Miyoshi, H., and Mantele, W. (1999) *Biochemistry* **38,** 14683–14689
16. Veselov, A. V., Osborne, J. P., Gennis, R. B., and Scholes, C. P. (2000) *Biochemistry* **39,** 3169–3175
17. Hastings, S. F., Heathcote, P., Ingledew, W. J., and Rigby, S. E. J. (2000) *Eur. J. Biochem.* **267,** 5638–5645
18. McMillan, F., Grimaldi, S., Ostermann, T., Weiden, N., Mogi, T., Ludwig, B., Miyoshi, H., Michel, H., and Prisner, T. F. (2003) *5th Meeting of the European Federation of EPR Groups*, Lisbon, Portugal, September 7–11, 2003
19. Grimaldi, S., Ostermann, T., Weiden, N., Mogi, T., Miyoshi, H., Ludwig, B., Michel, H., Prisner, T. F., and MacMillan, F. (2003) *Biochemistry* **42,** 5632–5639
20. Grimaldi, S., MacMillan, F., Ostermann, T., Ludwig, T., Michel, H., and Prisner, T. (2001) *Biochemistry* **40,** 1037–1043
21. Rumbley, J. N., Furlong Nickels, E., and Gennis, R. B. (1997) *Biochem. Biophys. Acta* **1340,** 131–142
22. Höfer, P., Grupp, A., Nebenführ, H., and Mehring, M. M. (1986) *Chem. Phys. Lett.* **132,** 279–284
23. Schweiger, A., and Jeschke, G. (2001) *Principles of Pulse Electron Paramagnetic Resonance*, pp. 359–405, Oxford University Press
24. Dikanov, S. A., and Bowman, M. K. (1995) *J. Magn. Reson. A* **116,** 125–128
25. MacMillan, F., Lendzian, F., and Lubitz, W. (1995) *Magn. Reson. Chem.* **33,** 581–593
26. Joela, H., Kasa, S., Lehtovuori, P., and Bech, M. (1997) *Acta Chem. Scand.* **51,** 233–241
27. Samoilova, R. I., van Liemt, W., Steggerda, W. F., Lugtenburg, J., Hoff, A. J., Spoyalov, A. P., Tyryshkin, A. M., Gritzan, N. P., and Tsvetkov, Yu.D. (1994) *J. Chem. Soc. Perkin Trans.* **2,** 609–614
28. Lubitz, W., and Feher, G. (1999) *Appl. Magn. Reson.* **17,** 1–49
29. McConnell, H. M. (1956) *J. Chem. Phys.* **24,** 764–768
30. Pedersen, J. A. (1985) *Handbook of EPR Spectra from Quinones and Quinols*, CRC Press, Boca Raton, FL, pp. 203–205
31. O'Malley, P. J., and Babcock, G. T. (1986) *J. Am. Chem. Soc.* **108,** 3995–4001
32. Flores, M., Isaacson, R. A., Calvo, R., Feher, G., and Lubitz, W. (2003) *Chem. Phys.* **294,** 401–413
33. Sinnecker, S., Reijerse, E., Neese, F., and Lubitz, W. (2004) *J. Am. Chem. Soc.* **126,** 3280–3290
34. Kasprzak, S., Kaupp, M., and MacMillam, F. (2006) *J. Am. Chem. Soc.*, **128,** 5661–5671
35. O'Malley, P. J. (1998) *Chem. Phys. Lett.* **291,** 367–374
36. Edmonds, D. T., and Speight, P. A. (1971) *Phys. Lett. A* **34,** 325–326
37. Blinc, R., Mali, M., Osredkar, R., Seliger, J., and Ehrenberg, L. (1974) *Chem. Phys. Lett.* **28,** 158–159
38. Ashby, C. I., Paton, W. F., and Brown, T. L. (1980) *J. Am. Chem. Soc.* **102,** 2990–2998
39. Rabbani, S. R., Edmonds, D. T., Gosling, P., and Palmer, M. H. (1987) *J. Magn. Reson.* **72,** 230–237
40. Dikanov, S. A., Tyryshkin, A. M., Felli, I., Reijerse, E. J., and Hüttermann, J. (1995) *J. Magn. Reson. B* **108,** 99–102
41. Palmer, M. H. (1984) *Z. Naturforsch. A* **39,** 1108–1111
42. Elmi, F., and Hadipour, N. L. (2005) *J. Phys. Chem. A*, **109,** 1729–1733
43. Spoyalov, A. P., Hulsebosch, R. J., Shochat, S., Gast, P., and Hoff, A. J. (1996) *Chem. Phys. Lett.* **263,** 715–720
44. Lendzian, F., Rautter, J., Käβ, H., Gardiner, A., and Lubitz, W. (1996) *Ber. Bunsenges. Phys. Chem.* **100,** 2036–2040
45. Deligiannakis, Y., Hanley, J., and Rutherford, A. W. (1999) *J. Am. Chem. Soc.* **121,** 7653–7664
46. Safin, I. A., and Osokin, D. Ya. (1977) *Nuclear Quadrupole Resonance in Nitrogen Compounds*, pp. 182–250, Science, Moscow